



MONTCLAIR STATE
UNIVERSITY

Montclair State University
**Montclair State University Digital
Commons**

Theses, Dissertations and Culminating Projects

12-2011

Escape Rates for Coupled Particles in a Stochastic Environment

Gregory Slusarczyk

Follow this and additional works at: <https://digitalcommons.montclair.edu/etd>



Part of the [Mathematics Commons](#)

MONTCLAIR STATE UNIVERSITY

ESCAPE RATES FOR COUPLED PARTICLES IN A
STOCHASTIC ENVIRONMENT

by

Gregory Slusarczyk

A Master's Thesis Submitted to the Faculty of

Montclair State University

In Partial Fulfillment of the Requirements

For the Degree of

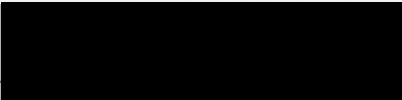
Master of Science in Mathematics, Pure and Applied Mathematics Concentration

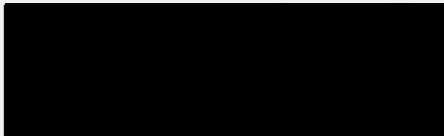
December 2011

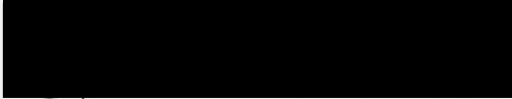
School College of Science and Mathematics

Thesis Committee:

Department Mathematical Sciences

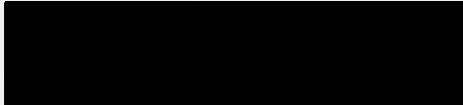

Dr. [Redacted]
Thesis Sponsor


Dr. Robert Prezant
Dean


Dr. Lora Billings

1/13/12
December 2011


Dr. Philip Yecko
Committee Member


Dr. Helen M. Roberts
Department Chair

ABSTRACT

Title of Thesis: ESCAPE RATES FOR COUPLED PARTICLES IN A
 STOCHASTIC ENVIRONMENT

Gregory Slusarczyk, Master of Science, 2011

Thesis directed by: Dr. Eric Forgoston
 Department of Mathematical Sciences

A particle placed in a deterministic, overdamped potential well will move towards an attractor located at the bottom of the well. Once the particle reaches the attractor, it remains there forever since no other forces are acting on the particle. However, if weak stochasticity is introduced, the particle will fluctuate around the attractor. As a rare event, the noise can organize itself in such a way that a large fluctuation is created that causes the particle to escape from the basin of attraction. The escape rates/escape times can be found both analytically and numerically. Furthermore, it is possible to predict the most probable trajectory of escape, called the optimal escape path, for the particle. In this work, we investigate the noise-induced escape of a single particle as well as two coupled particles from an overdamped double-well potential. For the coupled particles problem, we have developed new analytical tools needed to study the escape problem for different values of coupling, and our results are confirmed numerically.

ESCAPE RATES FOR COUPLED PARTICLES IN A
STOCHASTIC ENVIRONMENT

A THESIS

Submitted in partial fulfillment of the requirements

For the degree of Master of Science in Mathematics, Pure and Applied
Mathematics Concentration

By

GREGORY SLUSARCZYK

Montclair State University

Montclair, NJ

December 2011

Copyright c 2011 by *Gregory Slusarczyk*. All rights reserved.

Contents

1	Introduction	4
2	Single particle in a potential well	6
2.1	Theoretical escape time/escape rate	6
2.2	Application of theory to double-well potential	9
2.3	Comparison of analytical results with numerical simulation	11
3	Two coupled particles in a potential well	12
3.1	Theoretical escape time/escape rate: No coupling	15
3.2	Comparison of analytical results with numerical simulation: No coupling	15
3.3	Theoretical escape time/escape rate: Strong coupling	16
3.4	Comparison of analytical results with numerical simulation: Strong coupling	17
3.5	Theoretical escape time/escape rate: Weak / Intermediate coupling . .	19
3.6	Comparison of analytical results with numerical simulation: Weak / Intermediate coupling	21
3.7	Future work	22
4	Summary	25
	References	27

List of Figures

1	(a) Schematic diagram showing a particle in a quartic potential well. The particle fluctuates about the attractor located at the bottom of the well. After a long period of time, the noise causes the particle to escape from one basin of attraction to the other basin of attraction. (b) Numerical simulation showing the position of a particle in a quartic potential as a function of time. The particle fluctuates about the attractor located at $x = -1$ and after some finite period of time the particle escapes over the saddle located at $x = 0$ and starts oscillating about the other attractor located at $x = 1$	4
2	The double-well potential. The local minima are located at a and c , and the local maximum is located at b	7
3	Natural log of mean escape time vs $1/D$. The analytical line (blue) has slope $m = 0.25$, while the slope of the best fit line through the numerically computed data (red) is $m = 0.2583$	12
4	Natural log of mean escape time vs $1/D$. There is no coupling force between the particles. The analytical line (blue) has slope $m = 0.25$, while the slopes of the best fit lines through the numerically computed data for particle x_1 (red) and x_2 (green) are $m_1 = 0.25406$ and $m_2 = 0.25368$, respectively.	16
5	Natural log of mean escape time vs $1/D$. The coupling force between the particles is $k = 20$. The analytical line (blue) has slope $m = 0.4981$, while the slopes of the best fit lines through the numerically computed data for particle x_1 (red) and x_2 (green) are $m_{sc1} = 0.49931$ and $m_{sc2} = 0.49884$, respectively.	18
6	Natural log of mean escape time vs $1/D$. The coupling force between the particles ranges from $k = 1$ to $k = 20$. The analytical line (blue) has slope $m = 0.4981$. The slope of the best fit line through the numerically computed data for $k = 1$ for particle x_1 (red-triangles) is $m_1 = 0.4938$ and for x_2 (green-triangles) is $m_2 = 0.4939$, for $k = 2$ for particle x_1 (red-squares) is $m_1 = 0.5034$ and for x_2 (green-squares) is $m_2 = 0.5024$, for $k = 8$ for particle x_1 (red-stars) is $m_1 = 0.5037$ and for x_2 (green-stars) is $m_2 = 0.5024$, and for $k = 20$ for particle x_1 (red-dots) is $m_1 = 0.4993$ and for x_2 (green-dots) is $m_2 = 0.4988$	22
7	Mean escape time vs coupling for two particles. The asymptotic expansion (blue) is compared with the curves going through the numerically computed data points for x_1 (red) and x_2 (green).	23

List of Tables

1	Weak to intermediate couplings.	21
---	---	----

1 Introduction

When modeling physical and biological phenomena, it is often necessary to include the effect of stochasticity or noise on the system. Some of the fields that involve stochastic dynamical systems include epidemiology [4, 8, 9, 21], chemistry [19], biology [2], medicine [1], animal and robotic swarm behavior [11, 17], economics [14], and laser dynamics [5]. One important feature of many stochastic dynamical systems is the existence of a metastable state. In the absence of noise, these states are simply stable steady states. If weak noise is present, the system will fluctuate about this steady state. However, as a very rare event, the noise can organize itself and induce a large fluctuation that causes the system to escape from the metastable state. In many instances, the system will switch from one metastable state to another metastable state.

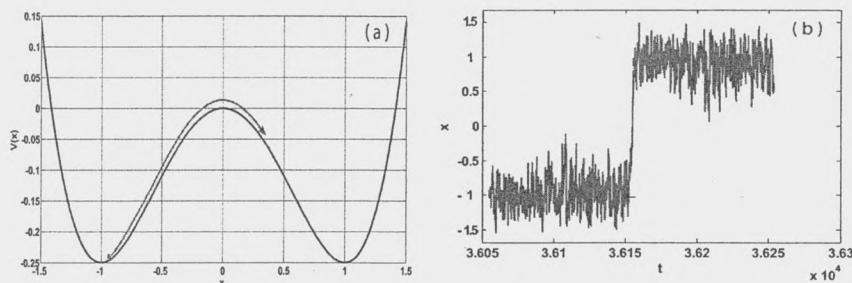


Figure 1: (a) Schematic diagram showing a particle in a quartic potential well. The particle fluctuates about the attractor located at the bottom of the well. After a long period of time, the noise causes the particle to escape from one basin of attraction to the other basin of attraction. (b) Numerical simulation showing the position of a particle in a quartic potential as a function of time. The particle fluctuates about the attractor located at $x = -1$ and after some finite period of time the particle escapes over the saddle located at $x = 0$ and starts oscillating about the other attractor located at $x = 1$.

Figure 1(a)-(b) reveals the behavior of a particle placed in a quartic potential well in the presence of a stochastic force. Figure 1(a) shows a schematic diagram of a particle placed in a double-well potential. The particle fluctuates at the bottom of the potential well about one of the attractors. After a long period of time, the noise causes the particle to escape to the other potential well. Figure 1(b) shows results from a numerical simulation. One can see the fluctuations of the particle about the attractor located at $x = -1$. As time progresses, a large fluctuation causes the particle to escape to the other potential well, where the particle starts to fluctuate about the other attractor located at $x = 1$. This switching from one metastable state to another metastable state can lead to significant changes in physical and biological systems. Several examples of noise-induced switching can be seen in nucleation at phase transitions [3], chemical reactions [16], protein transport in biological cells [6] and failures of electronic devices [18].

Although the outcome in all instances of escape is the same, as the particle switches from one metastable state to another metastable state, the actual path it takes to escape may be different for each event. However there is a path that is most likely to occur and we call this path the optimal escape path. Also there is a specific realization of noise associated with each specific path. In particular, the optimal escape path

has an associated optimal noise realization. Another important quantity that is often of interest is the escape rate from which one can find the escape time. Improving our knowledge of escape behavior leads to increased understanding of the fluctuation dynamics and ways of controlling the process.

For example, in epidemic modeling, stochasticity can cause a disease to go extinct. The stochastic fluctuations can arise from various sources and include internal noise due to the random interactions of individuals within a population, as well as external noise due to migration and fluctuations in birth rates. Typically, the number of infectious individuals in a population fluctuates about the metastable endemic state. As a rare event, and as described previously, the noise can organize itself to generate a large fluctuation that causes the disease to move away from the endemic state to the disease free state (i.e. extinct state). By determining the optimal path of escape/extinction as well as the escape rates, one can then employ control procedures to accelerate the process of extinction. In other words, by locating the optimal path, it is possible to use vaccine and other control measures to speed up extinction [8, 21].

The study of fluctuation dynamics that leads to escape of an object from a region of the ocean provides another example. The example is motivated by the need for profound understanding of processes governing the ocean dynamics. The processes have significant impact on weather, climate, marine fish and mammal populations, and contaminant transport [10], and therefore they are of great interest not only to basic science itself but also, due to its direct applications, to military and industry. However, to understand and predict the dynamics of such a complex environment, we need to constantly monitor the region of interest and gather data such as temperature, salinity and density. Scientists have used different devices for collecting these physical quantities, including surface drifters and submerged floats. One of the most promising are autonomous underwater gliders. In using these vehicles or sensors, one is often interested in positioning the glider in a particular monitoring region for long periods of time. Also of interest is the repositioning of a glider from one region to another region. Both of these require glider control. However, one of the major limitations of underwater gliders is the battery life. If one wishes to reduce the battery usage, one must reduce the amount of total control actuation that is used. To accomplish this, we will take advantage of the underlying structure of the stochastic ocean environment. The battery is used just to provide small corrections to maintain the desired course of the glider i.e. to keep it within a monitoring region of the ocean or to facilitate the escape from one region to another. As a first step, we shall consider a simplified model. Specifically, we consider a quartic potential that contains a particle subjected to stochastic noise. The particle represents the glider operating in the stochastic ocean, which is represented by the potential well. As a next step, we will investigate a collection of gliders whose members interact among each other. This collection can be seen as a robotic swarm [11, 17]. However, the investigation of a collection of hundreds or even tens of the gliders and their interaction parameters such as coupling or communication delay is extremely complex. Therefore we begin by introducing a system consisting only of two gliders and study the interaction between them in the presence of noise. For simplicity, the gliders will again be represented by two particles and the region of ocean will be substituted by an overdamped double-well potential.

The objective of this work is to formulate a general model that describes the dy-

namics of two coupled particles interacting with each other in a quartic potential and in the presence of noise. In particular we have determined analytically the escape rates of the particles for different regions of coupling, and we show that these results agree well with the numerically computed rates. Section 2 presents the general theory for both analytical and numerical results for one particle. In section 3, we extend our investigation to two coupled particles. We introduce analytical tools to study the escape problem and our results are confirmed numerically. Section 4 contains concluding remarks.

2 Single particle in a potential well

2.1 Theoretical escape time/escape rate

We consider the following first-order differential equation

$$\dot{x} = -\frac{dV(x)}{dx}, \quad (1)$$

where $V(x)$ represents a general potential function with multiple metastable states [12]. By adding a stochastic term $\sqrt{2D}\phi(t)$ to the deterministic differential equation given by Eq. (1), we obtain the Langevin equation

$$\dot{x} = -V'(x) + \sqrt{2D}\phi(t), \quad (2)$$

where $\phi(t)$ is a white stochastic force of intensity D that is characterized by the following correlation functions: $\langle\phi(t)\rangle = 0$ and $\langle\phi(t)\phi(t')\rangle = \delta(t-t')$.

As mentioned in Sec. 1, the noise can generate a large fluctuation that causes the system to switch from one metastable state to another. Thus we can expect in some finite time that the particle overcomes the barrier between metastable states and goes from one basin of attraction to another basin of attraction. This switching behavior can be observed in Fig. 1(b). At the initial time, the particle was placed near the left attractor. Figure 1(b) shows the stochastic fluctuations of the particle about that attractor. After some time, the noise organizes itself to create a large fluctuation that pushes the particle over the barrier and into the right basin of attraction. After descending into the right well, the particle fluctuates about the attractor for a long period of time.

The noise in the Langevin equation [Eq. (2)] can be expressed as

$$\phi(t) = \frac{\dot{x} + V'(x)}{\sqrt{2D}}. \quad (3)$$

Equation (3) shows that the stochastic term $\phi(t)$ can be written in terms of deterministic quantities. By applying Feynman's path integral formulation [7], it is possible to compute the probability of escape which is given by

$$P(x_{esc}) = \exp \left[- \int [\phi_{opt}(t)]^2 dt \right] = \exp \left[- \frac{1}{2D} \int [\dot{x} + V'(x)]^2 dt \right], \quad (4)$$

where $\phi_{opt}(t)$ represents the stochastic fluctuations associated with the optimal escape path [12]. To maximize the probability of the escape, the exponent of Eq. (4) has to be minimized. Using variational calculus [15], we know that x must satisfy the following Euler-Lagrange equation

$$L_x(t, x, \dot{x}) - \frac{d}{dt}L_{\dot{x}}(t, x, \dot{x}) = 0, \quad (5)$$

where the operator L is the Lagrangian given by

$$L(t, x, \dot{x}) = [\dot{x} + V'(x)]^2. \quad (6)$$

By solving Eq. (5), we can find the optimal escape path x_{esc} , and once it is known, we can use Eq. (3) to find the optimal noise $\phi_{opt}(t)$.

We can find the escape time/escape rate using the associated Fokker-Planck equation [13], which is given by

$$\partial_t p(x, t) = \partial_x [V'(x)p(x, t)] + D\partial_x^2 p(x, t), \quad (7)$$

where D represents the intensity of the noise, $V'(x)$ is the derivative of the potential function $V(x)$, and $p(x, t)$ denotes the probability that the particle is located at position x at time t . Since the particle sits for long periods of time in the bottom of the potential well before escape, we can assume that it is in a quasi-stationary state and therefore we may write $\partial_t p(x, t) = 0$. This means that the probability distribution p does not change in time. Therefore we can compute the mean escape time τ from one basin of attraction to another using Eq. (7) with $\partial_t p(x, t) = 0$ so that

$$\partial_x [V'(x)p(x, t)] + D\partial_x^2 p(x, t) = 0. \quad (8)$$

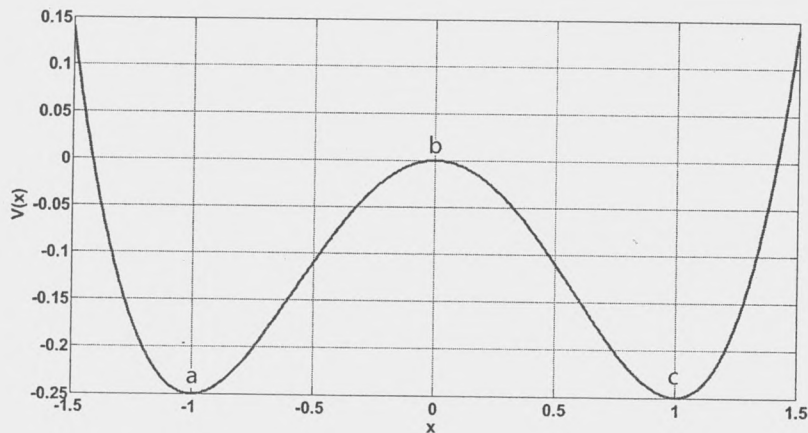


Figure 2: The double-well potential. The local minima are located at a and c , and the local maximum is located at b .

Integrating Eq. (8) twice, we can find the stationary probability distribution

$$\begin{aligned} p_s(x) &= \exp\left(-\frac{V(x)}{D}\right) \int \exp\left(\frac{V(x)}{D}\right) dx + C \exp\left(-\frac{V(x)}{D}\right) \\ &= C \exp\left(-\frac{V(x)}{D}\right) \end{aligned} \quad (9)$$

as well as the escape time

$$\tau = \frac{1}{D} \int_a^c \exp\left(\frac{V(x')}{D}\right) dx' \int_{-\infty}^{x'} \exp\left(-\frac{V(x'')}{D}\right) dx'', \quad (10)$$

where a , b and c are the local extrema of a quartic potential as shown in Fig. 2.

As $x' \rightarrow b$, $\exp\left(\frac{V(x')}{D}\right)$ increases (local maximum at $x' = b$, the saddle point). Employing a Taylor series expansion about b and evaluating at x' , we get

$$V(x') \approx V(b) + V'(b)(x' - b) + \frac{1}{2}V''(b)(x' - b)^2 = V(b) - \frac{1}{2}|V''(b)|(x' - b)^2 \quad (11)$$

where $V'(b)$ vanishes since $x' = b$ is the local maximum. Thus

$$\exp\left(\frac{V(x')}{D}\right) = \exp\left(\frac{V(b)}{D} - \frac{1}{2D}|V''(b)|(x' - b)^2\right). \quad (12)$$

For $x' \in (-\infty, b)$, $\int_{-\infty}^b \exp\left(-\frac{V(x'')}{D}\right) dx''$ has the largest contribution near $x'' = a$ (local minimum located at the bottom of a well). Therefore using a Taylor series expansion about a and evaluating at x'' , we obtain

$$\int_{-\infty}^{\infty} \exp\left(-\frac{V(a)}{D} - \frac{V''(a)}{2D}(x'' - a)^2\right) dx'', \quad (13)$$

and after some simple manipulation we get

$$\exp\left(-\frac{V(a)}{D}\right) \int_{-\infty}^{\infty} \exp\left[-\left(\frac{x'' - a}{\sqrt{\frac{2D}{V''(a)}}}\right)^2\right] dx''. \quad (14)$$

The above manipulation was done to express Eq. (13) in the form of a Gaussian integral given by Eq. (14). In general, the solution of a Gaussian integral is given by

$$\int_{-\infty}^{\infty} \exp(-kx^2) dx = \sqrt{\frac{\pi}{k}}. \quad (15)$$

Using Eq. (15) to evaluate Eq. (14) we find that

$$\begin{aligned} &\exp\left(-\frac{V(a)}{D}\right) \int_{-\infty}^{\infty} \exp\left[-\left(\frac{x'' - a}{\sqrt{\frac{2D}{V''(a)}}}\right)^2\right] dx'' \\ &= \exp\left(-\frac{V(a)}{D}\right) \sqrt{\frac{2\pi D}{V''(a)}}. \end{aligned} \quad (16)$$

Therefore Eq. (10) becomes

$$\tau = \frac{1}{D} \exp\left(-\frac{V(a)}{D}\right) \sqrt{\frac{2\pi D}{V''(a)}} \int_{-\infty}^{\infty} \exp\left(\frac{V(b)}{D} - \frac{(x' - b)}{\sqrt{\frac{2D}{V''(b)}}}\right)^2 dx'. \quad (17)$$

Evaluation of Eq. (17) leads to the following expression for the escape time

$$\begin{aligned} \tau &= \frac{1}{D} \sqrt{\frac{2\pi D}{V''(a)}} \sqrt{\frac{2\pi D}{|V''(b)|}} \exp\left(\frac{V(b) - V(a)}{D}\right) \\ &= \frac{2\pi}{\sqrt{V''(a)|V''(b)|}} \exp\left(\frac{V(b) - V(a)}{D}\right). \end{aligned} \quad (18)$$

The escape rate is given as

$$W(D) = \frac{1}{\tau} = \frac{\sqrt{V''(a)|V''(b)|}}{2\pi} \exp\left(-\frac{V(b) - V(a)}{D}\right). \quad (19)$$

2.2 Application of theory to double-well potential

In this section, we will apply the general theory from Sec. 2.1 to a specific example. We consider the following potential

$$V(x) = \frac{x^4}{4} - \frac{x^2}{2}. \quad (20)$$

With this potential Eq. (1) describes the behavior of a particle in a one-dimensional, overdamped double-well potential. The evolution equation of motion is

$$\dot{x} = x - x^3, \quad (21)$$

where \dot{x} and x respectively represent the velocity and position of the particle. In the deterministic case, when the particle is placed in the quartic potential given by Eq. (20), it will move 'downhill' to one of the local minima located at $x = \pm 1$ corresponding to stable equilibria. Once the particle reaches the minimum, it stays there forever due to the heavy damping [22].

Using Eq. (3), the noise is given by

$$\phi(t) = \frac{\dot{x} - x + x^3}{\sqrt{2D}}, \quad (22)$$

and the probability of escape is given by

$$P(x_{esc}) = \exp\left[-\frac{1}{2D} \int [\dot{x} - x + x^3]^2 dt\right], \quad (23)$$

where the integrand is the Lagrangian

$$L(t, x, \dot{x}) = [\dot{x} - x + x^3]^2. \quad (24)$$

Moreover, since the Lagrangian given by Eq. (24) does not depend explicitly on the independent variable t , the Euler-Lagrange equation given by Eq. (5) can be expressed as a first integral. The Euler-Lagrange equation is therefore

$$L(x, \dot{x}) - \dot{x}L_{\dot{x}}(x, \dot{x}) = 0, \quad (25)$$

which can be expanded to obtain

$$(\dot{x} - x + x^3)^2 - \dot{x} \frac{d}{dx} (\dot{x} - x + x^3)^2 = -\dot{x}^2 + x^2 - 2x^4 + x^6 = 0. \quad (26)$$

Simplifying, we obtain

$$\dot{x}^2 = x^2 - 2x^4 + x^6 = [x(x^2 - 1)]^2. \quad (27)$$

Using separation of variables, we solve Eq. (27). We begin with

$$\frac{dx}{dt} = x(x^2 - 1), \quad (28)$$

and rearrange to obtain

$$\int dt = \int \frac{dx}{x(x^2 - 1)}. \quad (29)$$

By employing the partial fractions technique, we get

$$\int dt = - \int \frac{dx}{x} + \int \frac{dx}{2(x-1)} + \int \frac{dx}{2(x+1)}. \quad (30)$$

Then after integrating the above equation, we obtain

$$t + c = -\ln|x| + \frac{1}{2}(\ln|x-1| + \ln|x+1|) = \ln \left| \frac{\sqrt{x^2 - 1}}{x} \right|, \quad (31)$$

and further simplification leads to

$$\exp(2t + c) = \frac{x^2 - 1}{x^2}. \quad (32)$$

In order to find the optimal escape path, we need to solve Eq. (32) for the variable x . After simple algebraic manipulation, we find that the optimal escape path is given by

$$x_{esc} = \pm \sqrt{\frac{1}{1 + \exp(2t)}}, \quad (33)$$

where the \pm sign denotes the initial location of the particle (minus for the left well and plus for the right one). Also we can clearly see that as $t \rightarrow -\infty$, $x_{esc} \rightarrow \pm 1$, the location of the attractors, and as $t \rightarrow \infty$, $x_{esc} \rightarrow 0$, the location of the saddle point.

The optimal noise is found using Eq. (3) to be

$$\phi_{opt} = \frac{\dot{x}_{esc} - x_{esc} + x_{esc}^3}{\sqrt{2D}}. \quad (34)$$

After substituting Eq. (33) into Eq. (34) and simplifying, we obtain

$$\phi_{opt}(t) = \frac{2 \exp(2t)}{(1 + \exp(2t))^{\frac{3}{2}}} \frac{1}{\sqrt{2D}}. \quad (35)$$

Using Eq. (20) we find the location of the potential well's extrema. The saddle point is located at $b = 0$ and the attractors at $a = -1$ and $c = 1$. The value of $V(0) = 0$ and $V(\pm 1) = -\frac{1}{4}$. Thus the depth of the potential well is $\Delta V = |V(b) - V(a)| = \frac{1}{4}$, $V''(b) = -1$, and $V''(a) = 2$.

Using these, Eq. (19) allows us to compute the escape rate as

$$W(D) = \frac{\sqrt{2}}{2\pi} \exp\left(-\frac{\Delta V}{D}\right) = \frac{\sqrt{2}}{2\pi} \exp\left(-\frac{1}{4D}\right). \quad (36)$$

The escape time is therefore

$$\frac{1}{W(D)} = \frac{2\pi}{\sqrt{2}} \exp\left(\frac{1}{4D}\right). \quad (37)$$

Taking the logarithm of both sides leads to the fact that

$$\ln\left(\frac{1}{W(D)}\right) = \ln\left(\frac{2\pi}{\sqrt{2}}\right) + \frac{1}{4D}. \quad (38)$$

2.3 Comparison of analytical results with numerical simulation

We now compare the analytical results with numerical simulation by numerically integrating the stochastic differential equation given by Eq. (2) using a fourth-order stochastic Runge-Kutta method with constant step size $h=0.001$. A particle was placed in the left basin of attraction near $x = -1$. Whenever noise caused the particle to escape to the other basin, the escape time was recorded. For our purposes, the escape time is the time it takes the particle to completely cross the barrier located at $x = 0$ (by completely, we mean the particle reaches the point $x = 0.2$, to be sure that it will not come back to the same basin of attraction it came from) or when the maximum time of 10^8 is exceeded.

The computation was done for 10,000 particles using the same noise intensity and the mean escape time was calculated. The process was repeated for a range of the noise intensity $D = \sigma^2/2$, by changing the standard deviation σ of the noise (σ runs from 0.3 to 0.6 with an increment size of 0.02). Figure 3 shows both analytical and numerical results of the natural log of the mean escape time vs $1/D$. A line of best fit was found for the numerically computed data, and the slope of the best fit line was calculated to be $m = 0.2583$.

There is excellent agreement between the slope of the best fit line through the numerically computed data and the slope obtained using the analytical method ($m = 0.25$). In Fig. 3, the vertical shift between these two lines is explained by the use of different conditions for escape. In the analytical derivation, the particle was required to reach the unstable saddle point at $x = 0$ to escape. However, for the numerical

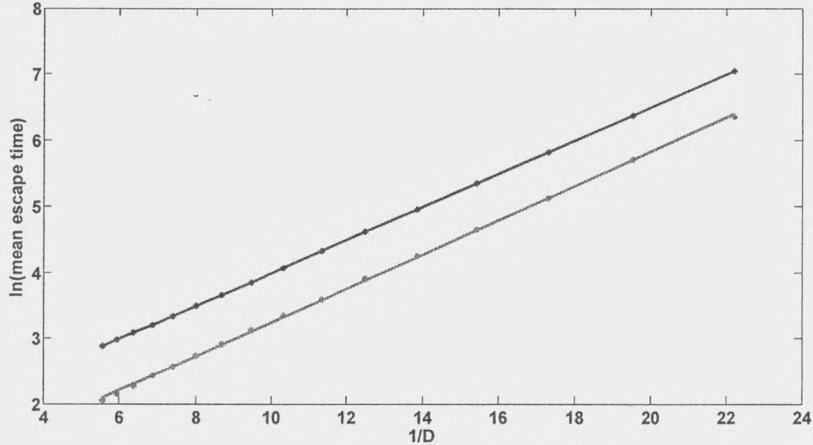


Figure 3: Natural log of mean escape time vs $1/D$. The analytical line (blue) has slope $m = 0.25$, while the slope of the best fit line through the numerically computed data (red) is $m = 0.2583$.

computation the particle had to travel over the saddle point and descend to $x = 0.2$ in order to escape.

3 Two coupled particles in a potential well

We now consider the case of two coupled particles interacting with each other in the presence of noise and in a double-well potential. In addition to the global well potential, we now need to consider the local potential due to the interaction between the coupled particles. To model the interaction between the particles, we use a spring potential given by

$$V_{sp} = \frac{k}{2}(x_1 - x_2 - l)^2, \quad (39)$$

where we assume that the mass of each particle is $m_1 = m_2 = 1$. In Eq. (39) k is a coupling parameter, l represents a distance parameter, and x_1 and x_2 denote the positions of the two particles. The force acting on the particles may change from being attractive to repelling and vice versa depending on the distance between the particles. In particular, if $|x_1 - x_2| < l$, the particles are repelled from each other, and if $|x_1 - x_2| > l$, the particles are attracted to one another. The total kinetic energy is

$$T(x_1, x_2) = \frac{1}{2}(\dot{x}_1^2 + \dot{x}_2^2), \quad (40)$$

where \dot{x}_1 and \dot{x}_2 represent the particle velocities.

Thus the total potential of the system is given as

$$\begin{aligned} V(x_1, x_2) &= V_{sp}(x_1, x_2) + V(x_1) + V(x_2) \\ &= \frac{k}{2}(x_1 - x_2 - l)^2 + V(x_1) + V(x_2). \end{aligned} \quad (41)$$

Equations (40) and (41) allow us to formulate the Lagrangian to be

$$\begin{aligned} L(x_1, x_2, \dot{x}_1, \dot{x}_2) &= T(x_1, x_2) - V(x_1, x_2) \\ &= \frac{\dot{x}_1^2 + \dot{x}_2^2}{2} - \frac{k}{2}(x_1 - x_2 - l)^2 - V(x_1) - V(x_2). \end{aligned} \quad (42)$$

The Euler-Lagrange equation is

$$\frac{d}{dt} \left(\frac{\partial L}{\partial \dot{x}_i} \right) - \left(\frac{\partial L}{\partial x_i} \right) = 0 \quad (43)$$

for $i = 1, 2$.

Solving Eq. (43), we get the system of equations

$$\ddot{x}_1 + k(x_1 - x_2 - l) + V'(x_1) = 0, \quad (44)$$

$$\ddot{x}_2 - k(x_1 - x_2 - l) + V'(x_2) = 0. \quad (45)$$

If we add damping terms, we obtain

$$\ddot{x}_1 + \alpha \dot{x}_1 + k(x_1 - x_2 - l) + V'(x_1) = 0, \quad (46)$$

$$\ddot{x}_2 + \alpha \dot{x}_2 - k(x_1 - x_2 - l) + V'(x_2) = 0. \quad (47)$$

In the case of an overdamped environment, the inertial terms \ddot{x}_1 and \ddot{x}_2 can be ignored. For simplicity we let $\alpha = 1$, and the system given by Eqs.(46) and (47) takes the form of the following governing equations:

$$\dot{x}_1 + k(x_1 - x_2 - l) + V'(x_1) = 0, \quad (48)$$

$$\dot{x}_2 - k(x_1 - x_2 - l) + V'(x_2) = 0. \quad (49)$$

The deterministic system of equations [Eq. (48) and Eq. (49)] can be made stochastic by adding noise terms, $\eta_1(t)$ and $\eta_2(t)$, to each of the governing equations to obtain

$$\dot{x}_1 = -k(x_1 - x_2 - l) - V'(x_1) + \eta_1(t) = F_1(x_1, x_2) + \eta_1(t), \quad (50)$$

$$\dot{x}_2 = k(x_2 - x_1 - l) - V'(x_2) + \eta_2(t) = F_2(x_1, x_2) + \eta_2(t). \quad (51)$$

As in the case of a single particle, we solve for $\eta_1(t)$ and $\eta_2(t)$ so that

$$\eta_1(t) = \dot{x}_1 - F_1(x_1, x_2), \quad (52)$$

$$\eta_2(t) = \dot{x}_2 - F_2(x_1, x_2), \quad (53)$$

which may be written in vector form as

$$\vec{\eta}(t) = \dot{\vec{x}} - \vec{F}(\vec{x}). \quad (54)$$

We again employ Feynman's path integral formulation [7], and compute the probability of the escape

$$P(x_{esc}) = \exp\left(-\int [\bar{\eta}(t)]^2 dt\right) = \exp\left(-\int \left[\dot{\vec{x}} - \vec{F}(\vec{x})\right]^2 dt\right), \quad (55)$$

where the Lagrangian is given by

$$L(\vec{x}, \dot{\vec{x}}) = \frac{1}{2} \left[\left\| \dot{\vec{x}} - \vec{F}(\vec{x}) \right\|^2 \right] = \frac{1}{2} \left[(\dot{x}_1 - F_1(x_1, x_2))^2 + (\dot{x}_2 - F_2(x_1, x_2))^2 \right] \quad (56)$$

Using Eq. (43), the Euler-Lagrange equations are

$$\frac{d}{dt} \left(\frac{\partial L}{\partial \dot{x}_1} \right) - \left(\frac{\partial L}{\partial x_1} \right) = 0, \quad (57)$$

$$\frac{d}{dt} \left(\frac{\partial L}{\partial \dot{x}_2} \right) - \left(\frac{\partial L}{\partial x_2} \right) = 0. \quad (58)$$

After substituting Eq. (56) into Eqs. (57) and (58) and simplifying, we obtain

$$\begin{aligned} \ddot{x}_1 &- \left[\frac{\partial F_1(x_1, x_2)}{\partial x_2} - \frac{\partial F_2(x_1, x_2)}{\partial x_1} \right] \dot{x}_2 - \\ &- \frac{\partial F_1(x_1, x_2)}{\partial x_1} F_1(x_1, x_2) - \frac{\partial F_2(x_1, x_2)}{\partial x_1} F_2(x_1, x_2) = 0, \end{aligned} \quad (59)$$

$$\begin{aligned} \ddot{x}_2 &- \left[\frac{\partial F_2(x_1, x_2)}{\partial x_1} - \frac{\partial F_1(x_1, x_2)}{\partial x_2} \right] \dot{x}_1 - \\ &- \frac{\partial F_1(x_1, x_2)}{\partial x_2} F_1(x_1, x_2) - \frac{\partial F_2(x_1, x_2)}{\partial x_2} F_2(x_1, x_2) = 0. \end{aligned} \quad (60)$$

Let's consider a specific example using the global potential given by Eq. (20). Since

$$F_1(x_1, x_2) = -k(x_1 - x_2 - l) - V'(x_1), \quad (61)$$

$$F_2(x_1, x_2) = k(x_1 - x_2 - l) - V'(x_2), \quad (62)$$

and

$$V'(x_1) = x_1^3 - x_1, \quad (63)$$

$$V'(x_2) = x_2^3 - x_2, \quad (64)$$

we therefore have

$$F_1(x_1, x_2) = -k(x_1 - x_2 - l) + x_1 - x_1^3, \quad (65)$$

$$F_2(x_1, x_2) = k(x_1 - x_2 - l) + x_2 - x_2^3. \quad (66)$$

Thus

$$\begin{aligned}\frac{\partial F_1(x_1, x_2)}{\partial x_2} &= k, \\ \frac{\partial F_2(x_1, x_2)}{\partial x_1} &= k, \\ \frac{\partial F_1(x_1, x_2)}{\partial x_1} &= -k + 1 - 3x_1^2, \\ \frac{\partial F_2(x_1, x_2)}{\partial x_2} &= -k + 1 - 3x_2^2.\end{aligned}$$

After a little algebra, Eqs.(59) and (60) become

$$\ddot{x}_1 - (-k + 1 - 3x_1^2)F_1(x_1, x_2) - kF_2(x_1, x_2) = 0, \quad (67)$$

$$\ddot{x}_2 - kF_1(x_1, x_2) - (-k + 1 - 3x_2^2)F_2(x_1, x_2) = 0. \quad (68)$$

3.1 Theoretical escape time/escape rate: No coupling

If we consider Eqs.(50) and (51) and set the coupling parameter k to zero, then we obtain

$$\dot{x}_1 = -V'(x_1) + \eta_1(t), \quad (69)$$

$$\dot{x}_2 = -V'(x_2) + \eta_2(t), \quad (70)$$

which clearly describes two independent (non-coupled) particles in a potential well. We can treat them separately, one at the time, so that our results for a single particle in a double-well potential can be applied (Section 2.1).

3.2 Comparison of analytical results with numerical simulation: No coupling

We numerically integrate the system of two stochastic differential equations given by Eqs. (50) and (51) with $k = 0$ using a fourth-order stochastic Runge-Kutta method with constant step size $h = 0.001$. Two particles were placed in the left basin of attraction. Whenever noise caused one of the particles to escape to the other basin (or if both escaped at the same time), the escape time was recorded. For our purposes, the escape time is the time it takes the particle to completely cross the barrier located at $x = 0$ (by completely, we mean the particle reaches the point $x = 0.2$, to be sure that it will not come back to the same basin of attraction it came from) or when the maximum time of 10^8 is exceeded.

The computation was done for 20,000 particles using the same noise intensity and the mean escape times for each of the particles was calculated. The process was repeated for a range of the noise intensity $D = \sigma^2/2$, by changing the standard deviation σ of the noise (σ runs from 0.3 to 0.6 with an increment size of 0.02). Figure 4 shows both analytical and numerical results of the natural log of the mean escape time vs. $1/D$. Lines of best fit were found for the numerically computed data for x_1 and x_2 , and the slopes of these lines were calculated to be $m_1 = 0.25406$ and $m_2 = 0.25368$, respectively.

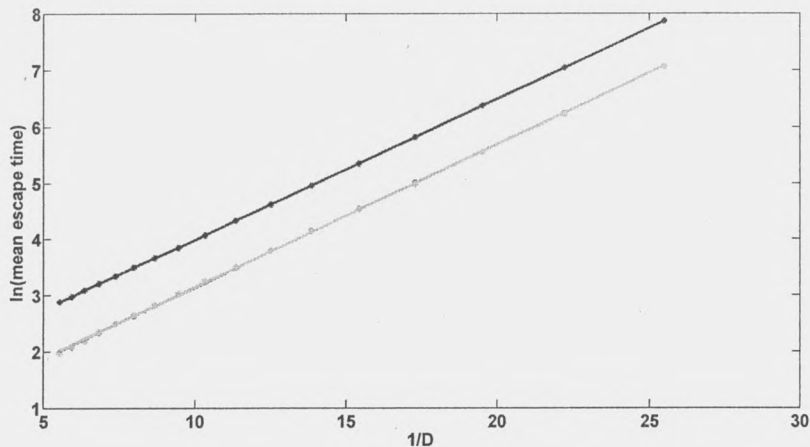


Figure 4: Natural log of mean escape time vs $1/D$. There is no coupling force between the particles. The analytical line (blue) has slope $m = 0.25$, while the slopes of the best fit lines through the numerically computed data for particle x_1 (red) and x_2 (green) are $m_1 = 0.25406$ and $m_2 = 0.25368$, respectively.

Figure 4 shows strong agreement between the numerically computed slopes m_1 and m_2 as well as the slope calculated in Section 2.1 using the analytical method ($m = 0.25$). The agreement is so strong that the best fit line for particle x_1 (red) is almost totally obscured by the best fit line for particle x_2 (green). The vertical shift between the two lines of best fit through the numerically computed data and the analytical line is explained by different conditions for escape. In the analytical derivation, the particle was required to reach the unstable saddle point at $x = 0$ to escape. However, for the numerical computation the particle had to travel over the saddle point and descend to $x = 0.2$ in order to escape.

3.3 Theoretical escape time/escape rate: Strong coupling

When the coupling between the particles is large, the distance between the two particles is approximately maintained at a constant equilibrium distance given by l . Therefore we can let $l = x_1 - x_2$ or $x_1 = x_2 + l$. If we denote $x_2 = x$ and $x_1 = x + l$ then the two-dimensional Eq. (41) can be rewritten as a one-dimensional potential. Thus we can apply the previously derived results for the escape time of one particle (Section 2.1). The only difference between the one particle and the two particle case is that the two particle case has a potential of the form $V(x) + V(x + l)$. Therefore, we expect

that the depth of the potential well in the strongly coupled two particle case will be different from the depth of the potential well in the one particle case. As a consequence of this difference, the mean escape times for both cases will differ as well.

If we consider the double-well potential example, Eq. (41) becomes

$$V(x) = \frac{k}{2}(0)^2 + \frac{(x+l)^4}{4} - \frac{(x+l)^2}{2} + \frac{x^4}{4} - \frac{x^2}{2}, \quad (71)$$

and therefore

$$V'(x) = (x+l)^3 + x^3 - 2x - l. \quad (72)$$

There are 4 roots of Eq. (71) given by

$$\begin{aligned} x = a &= \frac{-\sqrt{4-3l^2}-l}{2}, \\ x = b &= -\frac{l}{2}, \\ x = c &= \frac{\sqrt{4-3l^2}-l}{2} \end{aligned}$$

with corresponding extrema

$$\begin{aligned} V(a) &= \frac{1}{4}(-l^4 + 2l^2 - 2), \\ V(b) &= \frac{l^2}{32}(l^2 - 8), \\ V(c) &= \frac{1}{4}(-l^4 + 2l^2 - 2), \end{aligned}$$

where $x = b$ is a double root.

Thus for the specific value of parameter $l = 0.05$, we have local minima at $x = a = -1.0241$ and $x = c = 0.9741$ with value $V(a) = V(c) = \frac{1}{4}(-0.05^4 + 2 \cdot 0.05^2 - 2) = -0.4987$. Additionally, there is a local maximum at $x = b = 0.025$ with value $V(b) = \frac{0.05^2}{32}(0.05^2 - 8) = -0.0006$. The depth of the potential well is $\Delta V(x) = |V(b) - V(a)| = 0.4981$. Since $V''(x) = 3(x+l)^2 + 3x^2 - 2$, we have $V''(a) = 3.9925$ and $V''(b) = -1.9812$, and therefore, using Eq. (18), the escape time for the case of two strongly coupled particles is given by

$$\tau = \frac{2\pi}{\sqrt{V''(a)|V''(b)|}} \exp\left(\frac{\Delta V(x)}{D}\right) = 0.7943 \exp\left(\frac{0.4981}{D}\right). \quad (73)$$

3.4 Comparison of analytical results with numerical simulation: Strong coupling

We numerically integrate the system of two stochastic differential equations given by Eqs. (50) and (51) with $k = 20$ using a fourth-order stochastic Runge-Kutta method with constant step size $h = 0.001$. Two particles were placed in the left basin of

attraction. Whenever noise caused one of the particles to escape to the other basin (or if both escaped at the same time), the escape time was recorded. For our purposes, the escape time is the time it takes the particle to completely cross the barrier located at $x = 0$ (by completely, we mean the particle reaches the point $x = 0.2$, to be sure that it will not come back to the same basin of attraction it came from) or when the maximum time of 10^8 is exceeded.

The computation was done for 20,000 particles using the same noise intensity and the mean escape times for each of the particles was calculated. The process was repeated for a range of the noise intensity $D = \sigma^2/2$, by changing the standard deviation σ of the noise (σ runs from 0.3 to 0.6 with an increment size of 0.02). Figure 5 shows both analytical and numerical results of the natural log of the mean escape time vs $1/D$. Lines of best fit were found for the numerically computed data for x_1 and x_2 , and the slopes of these lines were calculated to be $m_{sc1} = 0.49931$ and $m_{sc2} = 0.49884$, respectively.

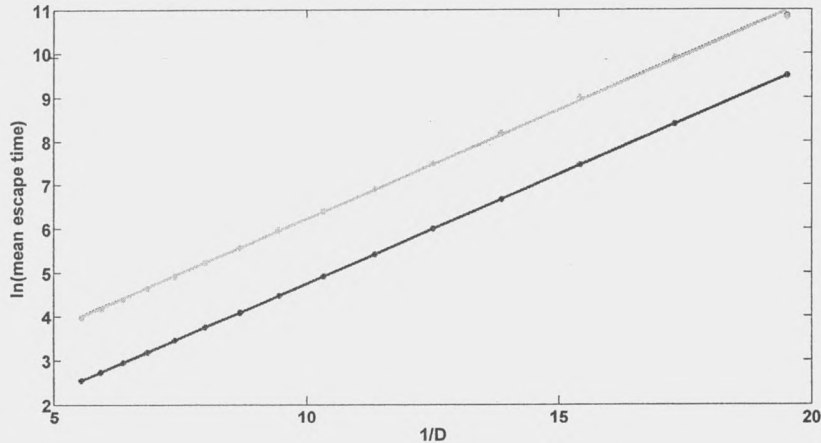


Figure 5: Natural log of mean escape time vs $1/D$. The coupling force between the particles is $k = 20$. The analytical line (blue) has slope $m = 0.4981$, while the slopes of the best fit lines through the numerically computed data for particle x_1 (red) and x_2 (green) are $m_{sc1} = 0.49931$ and $m_{sc2} = 0.49884$, respectively.

Figure 5 shows strong agreement between the numerically computed slopes m_{sc1} and m_{sc2} as well as the slope calculated in Section 3.3 using the analytical method ($m = 0.4981$). The agreement is so strong that the best fit line for particle x_1 (red) is almost totally obscured by the best fit line for particle x_2 (green). The vertical shift between the two lines of best fit through the numerically computed data and the analytical line is explained by different conditions for escape. In the analytical derivation, the particle was required to reach unstable saddle point at $x = 0$ to escape. However, for the numerical computation the particle had to travel over the saddle point and descend to $x = 0.2$ in order to escape.

3.5 Theoretical escape time/escape rate: Weak / Intermediate coupling

In this section we investigate coupling values that range from $k = 0.1$ to $k = 14$. To do this, we apply an asymptotic expansion to Eq. (41). First we differentiate Eq. (41) with respect to x_1 and x_2 , obtaining

$$\frac{\partial V(x_1, x_2)}{\partial x_1} = k(x_1 - x_2 - l) + V'(x_1), \quad (74)$$

$$\frac{\partial V(x_1, x_2)}{\partial x_2} = -k(x_1 - x_2 - l) + V'(x_2). \quad (75)$$

In order to find critical points we have to set each of the above equations equal to zero. Then if we divide Eqs. 74 and 75 by k and set $\epsilon = \frac{1}{k}$, we obtain

$$x_1 - x_2 - l + \epsilon V'(x_1) = 0, \quad (76)$$

$$-x_1 + x_2 + l + \epsilon V'(x_2) = 0, \quad (77)$$

where ϵ is treated as a perturbation parameter. We should note that the accuracy of our asymptotic expansion depends on the perturbation parameter in such a way that the smaller ϵ , the more accurate the results. Therefore, we can expect the best agreement for larger values of k .

We replace x_1 and x_2 in Eqs.(76) and (77) by the following power series

$$x_1 = a + \epsilon b + \epsilon^2 c + \dots, \quad (78)$$

$$x_2 = A + \epsilon B + \epsilon^2 C + \dots, \quad (79)$$

and by grouping the terms of the obtained equations with respect to the perturbation parameter ϵ , we get several systems of equations. Then we solve the systems for variables $a, b, c, \dots, A, B, C, \dots$ and substitute the solutions into Eq. (41) which in turn gives us values of local extrema of the potential $V(x_1, x_2)$. The difference between such a maximum and minimum gives the depth of the potential well $\Delta V(x_1, x_2)$.

We consider a particular example where the quartic potential is given by Eq. (20). Therefore Eqs.(76) and (77) become

$$x_1 - x_2 - l + \epsilon (x_1^3 - x_1) = 0 \quad (80)$$

$$-x_1 + x_2 + l + \epsilon (x_2^3 - x_2) = 0 \quad (81)$$

Then we replace x_1 and x_2 by the power series given by Eqs.(78) and (79). Thus Eq. (80) becomes

$$a + \epsilon b + \epsilon^2 c - A - \epsilon B - \epsilon^2 C - l + \epsilon \left[(a + \epsilon b + \epsilon^2 c)^3 - (a + \epsilon b + \epsilon^2 c) \right] = 0, \quad (82)$$

and Eq. (81) becomes

$$-a - \epsilon b - \epsilon^2 c + A + \epsilon B + \epsilon^2 C + l + \epsilon \left[(A + \epsilon B + \epsilon^2 C)^3 - (A + \epsilon B + \epsilon^2 C) \right] = 0. \quad (83)$$

Then we group terms from Eqs.(82) and (83) with respect to powers of perturbation parameter ϵ .

For $\mathcal{O}(0)$:

$$a = A + l. \quad (84)$$

For $\mathcal{O}(\epsilon)$:

$$a^3 - a + b - B = 0, \quad (85)$$

$$A^3 - A - b + B = 0. \quad (86)$$

For $\mathcal{O}(\epsilon^2)$:

$$3a^2 b - b + c - C = 0, \quad (87)$$

$$3A^2 B - B - c + C = 0. \quad (88)$$

For $\mathcal{O}(\epsilon^3)$:

$$3a^2 c + 3A^2 C + 3ab^2 + 3AB^2 - c - C = 0, \quad (89)$$

$$3a^2 c + 3A^2 C + 3ab^2 + 3AB^2 + c + C = 0. \quad (90)$$

Solving Eqs.(84)-(90) with $l = 0.05$, we get three roots. One represents the local maximum located at the saddle point, and the other two represent the local minima of the same value located at the bottom of the wells. For the maximum we have

$$a = \frac{1}{40}, \quad b = \frac{1599}{128000}, \quad c = \frac{-7670403}{654131200000},$$

$$A = -\frac{1}{40}, \quad B = -\frac{1599}{128000}, \quad C = \frac{7670403}{654131200000 \cdot 982},$$

and for the minimum

$$a = \frac{1 - \sqrt{1597}}{40}, \quad b = -\frac{399(1597 + 3\sqrt{1597})}{25552000}, \quad c = \frac{-477603(322391\sqrt{1597} + 2550409)}{6480079187200000},$$

$$A = \frac{-1 - \sqrt{1597}}{40}, \quad B = -\frac{399(-1597 + 3\sqrt{1597})}{25552000}, \quad C = \frac{-477603(322391\sqrt{1597} - 2550409)}{6480079187200000 \cdot 982}.$$

Replacing coefficients a, b, c, A, B, C by their actual values for the maximum roots in Eq. (78) and Eq. (79) and substituting the newly obtained x_1 and x_2 into Eq. (41), we get an asymptotic expansion, V_{max} , of Eq. (41) for the local maximum. If we repeat the procedure for the minimum roots, we get an asymptotic expansion, V_{min} , of Eq. (41) for the local minimum. Finally our potential well depth can be computed from $\Delta V = V_{max} - V_{min}$.

3.6 Comparison of analytical results with numerical simulation: Weak / Intermediate coupling

We numerically integrate the system of two stochastic differential equations given by Eqs. (50) and (51) with $k = 0.1$ to $k = 14$ using a fourth-order stochastic Runge-Kutta method with constant step size $h=0.001$. Two particles were placed in the left basin of attraction. Whenever noise caused one of the particles to escape to the other basin (or if both escaped at the same time), the escape time was recorded. For our purposes, the escape time is the time it takes the particle to completely cross the barrier located at $x = 0$ (by completely, we mean the particle reaches the point $x = 0.2$, to be sure that it will not come back to the same basin of attraction it came from) or when the maximum time of 10^8 is exceeded.

The computation was done for 20,000 particles using the same noise intensity and the mean escape times for each of the particles was calculated. The process was repeated for a range of the noise intensity $D = \sigma^2/2$, by changing the standard deviation σ of the noise (σ runs from 0.3 to 0.6 with an increment size of 0.02). Figure 6 shows both analytical and numerical results of the natural log of the mean escape time vs $1/D$ for $k = 1, 2, 8$, and 20, where lines of best fit were found for the numerically computed data for x_1 and x_2 . Slope values for other values of k can be found in Table 1.

k	Slope (asymptotic)	x_1 slope	Error %	x_2 slope	Error %
0.1	0.2522	0.2986	18.4	0.2978	18.1
0.2	0.4574	0.3388	25.9	0.3396	25.7
0.4	0.4906	0.4065	17.1	0.4063	17.2
0.6	0.4955	0.4529	8.6	0.4528	8.6
0.8	0.4969	0.4790	3.6	0.4796	3.5
1	0.4976	0.4938	0.8	0.4939	0.7
2	0.4982	0.5034	1	0.5024	0.8
4	0.4983	0.5079	1.9	0.5068	1.7
6	0.4982	0.5053	1.4	0.5043	1.2
8	0.4982	0.5037	1.1	0.5024	0.8
10	0.4982	0.5026	0.9	0.5016	0.7
12	0.4982	0.5012	0.6	0.5002	0.4
14	0.4982	0.5010	0.6	0.5002	0.4

Table 1: Weak to intermediate couplings.

The second column of Table 1 shows analytical values of the slope computed using the asymptotic expansion of the potential well for different coupling values (column 1). The third and fifth columns indicate the numerically obtained slopes of the lines of best fit of x_1 and x_2 , respectively. The fourth and sixth columns give the relative error between the analytical and numerical results. Based on the relative errors, we can observe excellent agreement between the numerically and analytically obtained slopes for the intermediate coupling values ($k = 1$ to $k = 14$). However, the relative error for the weak coupling values ($k = 0.1$ to $k = 0.8$) shows that there is not good

agreement between the analytical and numerical results. The poor agreement is due to the perturbation parameter ϵ being too large. Therefore, to analytically find the escape times for the case of weak coupling we need to develop another analytical method.

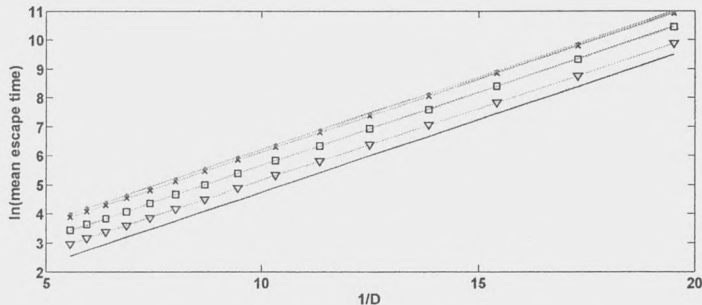


Figure 6: Natural log of mean escape time vs $1/D$. The coupling force between the particles ranges from $k = 1$ to $k = 20$. The analytical line (blue) has slope $m = 0.4981$. The slope of the best fit line through the numerically computed data for $k = 1$ for particle x_1 (red-triangles) is $m_1 = 0.4938$ and for x_2 (green-triangles) is $m_2 = 0.4939$, for $k = 2$ for particle x_1 (red-squares) is $m_1 = 0.5034$ and for x_2 (green-squares) is $m_2 = 0.5024$, for $k = 8$ for particle x_1 (red-stars) is $m_1 = 0.5037$ and for x_2 (green-stars) is $m_2 = 0.5024$, and for $k = 20$ for particle x_1 (red-dots) is $m_1 = 0.4993$ and for x_2 (green-dots) is $m_2 = 0.4988$.

In Fig. 6 we can observe such strong agreement between the best fit line of x_1 and x_2 that the lines overlap. Also the parallel orientation of the lines shows close agreement between the slopes of the lines. Notice that with increasing the coupling, the lines shift upwards. The vertical shifts between analytical line and numerical ones can be explained by different escape conditions, just like it was in previous sections. However, the shifts between numerical lines is due to the fact that with increasing the coupling, it is harder to escape and therefore the mean escape times increase. The vertical shift decreases as the value of coupling increases. Beyond the strong coupling value of $k = 20$, the results are nearly identical.

Figure 7 shows that once we cross the intermediate-strong threshold of $k = 14$, the mean escape times obtained from numerical computations converge to the value of 0.4981 which is the analytical slope for strong coupling. Also Fig. 7 confirms the observation made in discussing the data from Table 1 that the weak-intermediate threshold is located near $k = 1$.

3.7 Future work

To properly capture the escape rates/times for weak coupling, we recently derived in an alternate fashion the governing equations that maximize the escape probability. The method involves a variational approach that uses Lagrange multipliers. The method is general and allows one to find the optimal escape path as well as the escape rate.

We begin by demonstrating the procedure for the single particle problem given by

$$\dot{x}(t) = F(x(t)) + \xi(t). \quad (91)$$

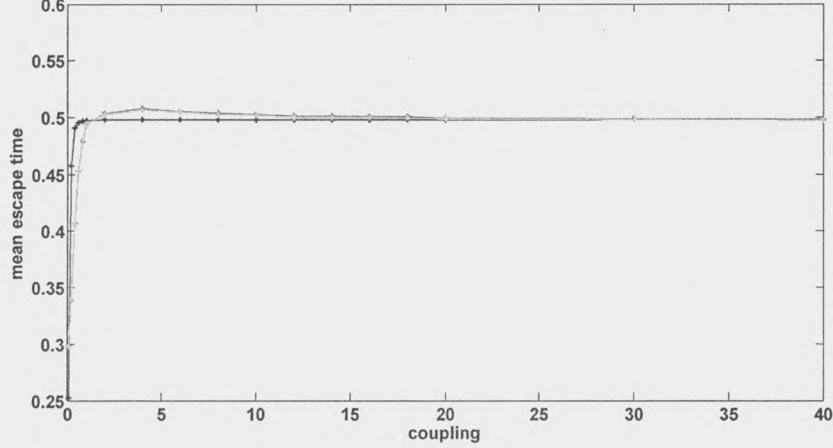


Figure 7: Mean escape time vs coupling for two particles. The asymptotic expansion (blue) is compared with the curves going through the numerically computed data points for x_1 (red) and x_2 (green).

The probability of a large fluctuation [20] is given by

$$P_x[x] = \exp\left(-\frac{R}{D}\right), \quad (92)$$

where $R = \min \mathcal{R}[x, \xi, \lambda]$, and

$$\begin{aligned} \mathcal{R}[x, \xi, \lambda] &= \mathcal{R}_\xi[\xi(t)] + \int \lambda(t)[\dot{x}(t) - F(x) - \xi(t)]dt \\ &= \frac{1}{2} \int \xi^2(t)dt + \int \lambda(t)[\dot{x}(t) - F(x) - \xi(t)]dt. \end{aligned} \quad (93)$$

To determine the exponent \mathcal{R} , we seek the equations that describe the maximum probability of reaching the saddle if we start at the attractor. We derive the variation $\delta\mathcal{R}$ by varying deviations from the path that minimizes \mathcal{R} .

First, we consider the variation with respect to noise ξ . Therefore we get

$$\begin{aligned} \frac{\delta\mathcal{R}}{\delta\xi} &= \mathcal{R}[x, \xi + \eta, \lambda] - \mathcal{R}[x, \xi, \lambda] \\ &= \left[\frac{1}{2} \int (\xi + \eta)^2 dt + \int \lambda [\dot{x} - F - (\xi + \eta)] dt \right] \\ &\quad - \left[\frac{1}{2} \int \xi^2 dt + \int \lambda [\dot{x} - F - \xi] dt \right] \\ &= \frac{1}{2} \int [(\xi + \eta)^2 - \xi^2] dt - \int \lambda [(\xi + \eta) - \xi] dt \\ &= \frac{1}{2} \int 2\xi\eta + \eta^2 dt - \int \lambda\eta dt = \int (\xi - \lambda)\eta dt + \mathcal{O}(\eta^2). \end{aligned} \quad (94)$$

Since η is an arbitrary smooth function, we get

$$\lambda = \xi. \quad (95)$$

Now we consider the variation with respect to the Lagrange multiplier λ . The equation is

$$\begin{aligned}
\frac{\delta \mathcal{R}}{\delta \lambda} &= \mathcal{R}[x, \xi, \lambda + \eta] - \mathcal{R}[x, \xi, \lambda] \\
&= \left[\frac{1}{2} \int \xi^2 dt + \int (\lambda + \eta) [\dot{x} - F - \xi] dt \right] \\
&\quad - \left[\frac{1}{2} \int \xi^2 dt + \int \lambda [\dot{x} - F - \xi] dt \right] \\
&= \int (\lambda - \lambda + \eta) [\dot{x} - F - \xi] dt = \int \eta [\dot{x} - F - \xi] dt.
\end{aligned} \tag{96}$$

Thus

$$\dot{x} - F - \xi = 0 \Rightarrow \dot{x} = F + \xi. \tag{97}$$

Finally we consider the variation with respect to x . We have

$$\begin{aligned}
\frac{\delta \mathcal{R}}{\delta x} &= \mathcal{R}[x + \eta, \xi, \lambda] - \mathcal{R}[x, \xi, \lambda] \\
&= \left[\frac{1}{2} \int \xi^2 dt + \int \lambda [\dot{x} + \dot{\eta} - F(x + \eta) - \xi] dt \right] \\
&\quad - \left[\frac{1}{2} \int \xi^2 dt + \int \lambda [\dot{x} - F(x) - \xi] dt \right] \\
&= \int \lambda [\dot{\eta} + F(x) - F(x + \eta)] dt \\
&= - \int \dot{\lambda} \eta + \lambda \frac{\delta F}{\delta x} \eta dt \\
&= - \int \eta \left[\dot{\lambda} + \lambda \frac{\delta F}{\delta x} \right] dt.
\end{aligned} \tag{98}$$

Thus

$$- \left[\dot{\lambda} + \lambda \frac{\delta F}{\delta x} \right] = 0. \tag{99}$$

Equations (95), (97), and (99) form the following system of ordinary differential equations

$$\begin{aligned}
\dot{x} &= \lambda + F(x), \\
\dot{\lambda} &= -\lambda \frac{\delta F}{\delta x}.
\end{aligned} \tag{100}$$

By solving the system of equations given by Eq. (100), we get the following set of equations which can be solved to find the optimal escape path and escape rates.

$$\begin{aligned}
\lambda &= -2F(x), \\
\dot{x} &= -F(x).
\end{aligned} \tag{101}$$

We can extend the above derivation to the two particles problem given by

$$\dot{\vec{x}} = \vec{F}(\vec{x}) + \vec{\xi}(t). \quad (102)$$

Now

$$\begin{aligned} \mathcal{R} [\vec{x}, \vec{\xi}, \vec{\lambda}] &= \mathcal{R}_\xi[\xi] + \int \vec{\lambda} \left[\dot{\vec{x}} - \vec{F}(\vec{x}) - \vec{\xi} \right] dt \\ &= \frac{1}{2} \int \xi_1^2 + \xi_2^2 dt + \int \vec{\lambda} \cdot \left[\dot{\vec{x}} - \vec{F}(\vec{x}) - \vec{\xi} \right] dt \end{aligned} \quad (103)$$

If

$$\begin{aligned} \dot{x}_1 &= F_1(x_1, x_2) + \xi_1 \\ \dot{x}_2 &= F_2(x_1, x_2) + \xi_2 \end{aligned} \quad (104)$$

then

$$\begin{aligned} &\mathcal{R} [\langle x_1, x_2 \rangle, \langle \xi_1, \xi_2 \rangle, \langle \lambda_1, \lambda_2 \rangle] \\ &= \frac{1}{2} \int \xi_1^2 + \xi_2^2 dt + \int \langle \lambda_1, \lambda_2 \rangle \cdot \langle \dot{x}_1 - F_1 - \xi_1, \dot{x}_2 - F_2 - \xi_2 \rangle dt \\ &= \frac{1}{2} \int \xi_1^2 + \xi_2^2 dt + \int \lambda_1 (\dot{x}_1 - F_1 - \xi_1) + \lambda_2 (\dot{x}_2 - F_2 - \xi_2) dt \end{aligned} \quad (105)$$

Now if we consider the variations with respect to $\xi_1, \xi_2, x_1, x_2, \lambda_1, \lambda_2$, we obtain the following

$$\begin{aligned} \lambda_1 &= \xi_1, \\ \lambda_2 &= \xi_2, \\ \dot{x}_1 &= F_1 + \xi_1, \\ \dot{x}_2 &= F_2 + \xi_2, \\ 0 &= -\dot{\lambda}_1 - \lambda_1 \frac{\delta F_1}{\delta x_1} - \lambda_2 \frac{\delta F_2}{\delta x_1}, \\ 0 &= -\dot{\lambda}_2 - \lambda_1 \frac{\delta F_1}{\delta x_2} - \lambda_2 \frac{\delta F_2}{\delta x_2}. \end{aligned}$$

Unlike the single particle case, this system doesn't have an analytical solution. Therefore, we must solve the system numerically. For example, we may use a shooting method. This is non-trivial in high-dimensions and we are currently working on this numerical problem. The solution, as in the single particle case, will enable us to find the optimal escape and escape times for every parameter and coupling value of interest.

4 Summary

We have studied the dynamics of a single particle placed in an overdamped double-well potential. Due to a stochastic force, the particle fluctuates for most of the time

around an attractor located at the bottom of the well. However, as a rare event, the noise generates a large fluctuation that causes the escape of the particle to the other well. We analytically derived the expression for escape rates and escape times for the particle and showed there is a linear relationship between the mean escape time and the inverse of the noise intensity. Furthermore, our analytical results were confirmed by numerical computations.

We then extended the theory and derived analytical expressions for the escape time and escape rate for two coupled particles placed in an overdamped potential well in the presence of stochastic noise. As a starting point in our derivation, we used a spring potential for the local interaction and a global double-well potential. The analysis was performed for different values of the coupling parameter.

First, we considered the case of no coupling between two particles. In this case, the particles will behave as two independent systems, and therefore the single particle theory can be used. We saw excellent agreement between the slopes of the best fit lines from the numerical simulation and the analytical slope of the line, given by the depth of the potential well.

Next, we investigated the case of strong coupling, assuming this time that the coupling force between the particles is so strong that repulsive and contracting forces are approximately in equilibrium. Therefore, the distance between the particles did not change and we could treat the particles as a special case of the one particle theory. The analytically obtained depth of the potential well was in good agreement with the slopes of the best fit lines from the numerical simulation.

For the third case of weak to intermediate coupling, we had to develop different analytical tools to find the escape time. We employed an asymptotic expansion with respect to $1/k$. This approach gave the mean escape time for intermediate coupling values ($k=1$ to $k=14$) that compared very favorably with numerical simulation. The relative error between the asymptotic expansion results and numerical results for the above range of coupling values was less than 1.9 % and became even lower for higher coupling values in the range. However, for the weak coupling values ($k=0.1$ to $k=0.8$), the agreement between the analytical and numerical results is not as good. Therefore, to solve this problem, we proposed a new analytical method in Section 3.7. that will enable us to find the optimal escape path and the escape time for all parameter and coupling values.

There is much more work to be done. Of interest is the inclusion of more particles as well as the extension to simple, but realistic ocean flows, and continuing on to more complicated ocean flows. The results presented here and future results will provide the first steps in understanding how to optimally use autonomous underwater gliders for monitoring ocean regions as well as in understanding switching behavior in other physical and biological systems.

References

- [1] A.A. Armoundas, K. Ju, N. Iyengar, J.K. Kanters, P.J. Saul, R.J. Cohen, and K.H. Chon. A stochastic nonlinear autoregressive algorithm reflects nonlinear dynamics of heart-rate fluctuations. *Annals of Biomedical Engineering*, 30(2):192–201, 2002.
- [2] E.A. Arriaga. Determining biological noise via single cell analysis. *Analytical and Bioanalytical Chemistry*, 393(1):73–80, 2009.
- [3] V. Basso, C. Beatrice, G. Bertotti, G. Durin, M. Lo Bue, and C.P. Sasso. Barkhausen noise in nucleation-type hard magnetic materials. *Journal of Magnetism and Magnetic Materials*, 272-276:E539–E541, 2004.
- [4] L. Billings, E. Bollt, and I.B. Schwartz. Phase-space transport of stochastic chaos in population dynamics of virus spread. *Physical Review Letters*, 88:234101, 2002.
- [5] B.C. Buchler, E.H. Huntington, C.C. Harb, and T.C. Ralph. Feedback control of laser intensity noise. *Physical Review A*, 57(2):1286–1294, 1998.
- [6] P. Carlini, A. R. Bizzarri, and S. Cannistraro. Temporal fluctuations in the potential energy of proteins: $1/f^\alpha$ noise and diffusion. *Physica D: Nonlinear Phenomena*, 165(3-4):242 – 250, 2002.
- [7] R. Feynman and A. Hibbs. *Quantum Mechanics and Path Integrals*. McGraw-Hill, New York, 1965.
- [8] E. Forgoston, S. Bianco, L.B. Shaw, and I.B. Schwartz. Maximal sensitive dependence and the optimal path to epidemic extinction. *Bulletin of Mathematical Biology*, 73(3):495–514, 2011.
- [9] E. Forgoston, L. Billings, and I.B. Schwartz. Accurate noise projection for reduced stochastic epidemic models. *Chaos*, 19:043110, 2009.
- [10] E. Forgoston, L. Billings, P. Yecko, and I.B. Schwartz. Set-based corral control in stochastic dynamical systems: Making almost invariant sets more invariant. *Chaos*, 21:013116, 2011.
- [11] E. Forgoston and I.B. Schwartz. Delay-induced instabilities in self-propelling swarms. *Physical Review E*, 77:035203(R), 2008.
- [12] E. Forgoston and I.B. Schwartz. Escape rates in a stochastic environment with multiple scales. *SIAM Journal on Applied Dynamical System*, 8:1190–1217, 2009.
- [13] W. Gardiner. *Handbook of Stochastic Methods for Physics, Chemistry and the Natural Sciences*. Springer-Verlag, New York, 2004.
- [14] J. Li and S. Li. Dynamics of a business cycle model under harmonic and stochastic noise excitation. *Far East Journal of Applied Mathematics*, 38(2):119–129, 2010.
- [15] J. Logan. *Applied Mathematics*. Wiley, New York, 1997.

- [16] F. Marchesoni. Thermally activated chemical reactions in the presence of internal multiplicative noise. *Chemical Physics Letters*, 110(1):20 – 24, 1984.
- [17] L. Mier-y Teran-Romero, E. Forgoston, and I.B. Schwartz. Noise, bifurcations, and modeling of interacting particle systems. In *Proceedings of the 2011 IEEE/RSJ International Conference on Intelligent Robots and Systems (IROS)*, 3905–3910, 2011.
- [18] Ch. Prakash. Analysis of non-catastrophic failures in electronic devices due to random noise. *Microelectronics Reliability*, 16(5):587 – 588, 1977.
- [19] K. Rohlf. Stochastic phase-space description for reactions that change particle numbers. *Journal of Mathematical Chemistry*, 45(1):141–160, 2009.
- [20] I. B. Schwartz, T. W. Carr, L. Billings, and M. Dykman. Stochastic extinction in non-gaussian environments with differential delay. In preparation, 2011.
- [21] I.B. Schwartz, E. Forgoston, S. Bianco, and L.B. Shaw. Converging towards the optimal path to extinction. *Journal of the Royal Society Interface*, 8(65):1699–1707, 2011.
- [22] S. Strogatz. *Nonlinear Dynamics and Chaos*. Westview Press, Cambridge, 2001.